Available online at www.sciencedirect.com

SciVerse ScienceDirect

journal homepage: www.elsevier.com/locate/he

Comparative study on MoS_2 and WS_2 for electrocatalytic water splitting

Tzu-Yin Chen [a,1], Yung-Huang Chang [a,1], Chang-Lung Hsu [b], Kung-Hwa Wei [b], Chia-Ying Chiang [a,*], Lain-Jong Li [a,c,**]

[a] Institute of Atomic and Molecular Sciences, Academia Sinica, Taipei 10617, Taiwan
[b] Department of Materials Science & Engineering, National Chiao Tung University, HsinChu 300, Taiwan
[c] Department of Medical Research, China Medical University Hospital, Taichung, Taiwan

ARTICLE INFO

Article history:
Received 6 March 2013
Received in revised form
4 July 2013
Accepted 7 July 2013
Available online 7 August 2013

Keywords:
Hydrogen evolution reaction
Electrocatalytic reaction
Molybdenum disulfide
Tungsten disulfide

ABSTRACT

Replacing Pt by earth abundant catalysts is one of the most important tasks toward potential large-scale HER applications. Among many potential candidates, low cost and earth abundant transition metal dichalcogenides such as MoS_2 and WS_2 have been promising as good H_2 evolution electrocatalysts when they are engineered into the structures with active sites. In this work, we have performed systematic studies on the catalytic reactivity of both MoS_2 and WS_2 materials produced by one-step and scalable thermolysis from $(NH_4)_2WS_4$ and $(NH_4)_2MoS_4$ precursors respectively. Structural analysis shows that these materials prepared at a higher thermolysis temperature exhibit higher crystallinity. The H_2 evolution electrocatalysts efficiency for the MoS_2 prepared at a lower temperature is higher than those at higher temperatures, where amorphous MoS_2 or S_2^{2-} species instead of crystalline MoS_2 is the main active site. By contrast, crystalline WS_2 prepared at high temperature is identified to be the key reaction site. Both catalysts display excellent efficiency and durability as an electrocatalyst operating in acidic electrolytes. This work provides fundamental insights for further design and preparation of emergent metal dichalcogenide catalysts, beneficial for the development in clean energy.

1. Introduction

Due to the rapid depletion of the carbon based fuels and their environmental contaminations, an enormous worldwide demand for an alternative clean energy is being vigorously pursued. Hydrogen is thus an ideal energy carrier because there is no green house gas such as carbon dioxide (CO_2) emitted during the combustion process. Particularly, sustainable hydrogen production from electrolytic water splitting has gained more and more attention [1–12] since the conversion of solar to electrical energy by a photovoltaic cell is mature in industry. This water splitting reaction is known as the hydrogen evolution reaction (HER). In order to increase the efficiency of HER, i.e. mainly by lowering the reaction overpotential, a highly active catalyst is essential. Based on the volcano plot [13], Pt possesses an almost zero overpotential for HER; however it is not a favorable candidate for HER because of its high cost and rareness on earth.

* *Corresponding author*. Tel.: +886 2 23668264.
** *Corresponding author*. Institute of Atomic and Molecular Sciences, Academia Sinica, Taipei 10617, Taiwan. Tel.: +886 2 23668205.
E-mail addresses: cychiang@gate.sinica.edu.tw (C.-Y. Chiang), lanceli@gate.sinica.edu.tw (L.-J. Li).
[1] These authors contributed equally.

0360-3199/$ – see front matter
http://dx.doi.org/10.1016/j.ijhydene.2013.07.021

As a result, the scientific community has been eagerly searching for an inexpensive and earth abundant substitution. Studies of density functional theory (DFT) on catalyst-hydrogen binding energy have shown that molybdenum disulfide (MoS_2) locates close to the top of the volcano curve [13]. The capability of MoS_2 for serving as a HER catalyst was subsequently verified by electrochemical measurements [14–26]. More importantly, a widely used industrial catalyst, MoS_2, costs much lower than the Pt. Due to its structural and electronic similarities to MoS_2, tungsten disulfide (WS_2) has also received some attention as an electrocatalyst recently [27,28]. However, to date most of the reports deal with hydrogen evolution reaction (HER) either with amorphous or single crystal MoS_2. Also, only very few papers deal with HER employing WS_2-based materials. The systematic study for these materials is still lacking. Hence it is important to explore the fundamentals, in particular the structure-HER property for these emergent materials.

Liu and his coworkers have demonstrated that the thermolysis of ammonium tetrathiomolybdate ($(NH_4)_2MoS_4$) in a chemical vapor deposition (CVD) furnace is able to produce high-quality MoS_2 thin layers [29]. In this work, we synthesized WS_2 and MoS_2 from the thermolysis of $(NH_4)_2WS_4$ and $(NH_4)_2MoS_4$ precursors respectively on carbon cloth. The reason for choosing CVD thermolysis as the method for producing these materials is that it is a one-step synthesis for MoS_2 and WS_2 and it also has the potential to serve for the large scale production. Carbon cloth is selected as the conducting substrate for loading these catalysts due to its fairly high surface area. This study demonstrated that the WS_2 catalyst prepared at high temperature has better performance than that prepared a lower thermolysis temperature, whereas the MoS_2 formed at lower temperature shows better HER efficiency. Our HER results, spectroscopic and structural analysis show that crystalline WS_2 is the active catalyst, which is in clear contrast to the MoS_2 system where amorphous MoS_2 or S_2^{2-} species is the key component for HER.

2. Material and method

2.1. Preparation of WS_2 and MoS_2

The preparation of WS_2 and MoS_2 is schematically illustrated in Fig. 1(a). Carbon cloth (W0S1002 from CeTech) was used as the conducting substrate to load the precursors, i.e. ammonium tetrathiotungstate solution ($(NH_4)_2WS_4$ (Alfa Aesa 99.9%); 5 wt% in dimethylformamide) or ammonium tetrathiomolybdate solution ($(NH_4)_2MoS_4$ (Alfa Aesa 99.99%); 5 wt% in dimethylformamide). The loading amounts for MoS_2 and WS_2 on carbon cloth are 2.6 and 14 mg/cm^2, respectively. After loading the precursors by immersion, carbon cloth was then baked on a hot-plate at 100 °C for 10 min. The precursor-coated substrates were then fed into a tube furnace for thermolysis and the standard environment was kept at 500 torr with the gas mixture of for H_2 and Ar (20 and 80 sccm respectively) unless specified in text. WS_2 and MoS_2 were subsequently formed on the carbon cloth at various temperatures set for thermolysis [29,30].

2.2. Characterization

X-ray diffraction patterns were obtained with a Philips PANalytical X'Pert MPD using Cu Kα (0.154 nm) as incident radiation. It was operated at 45 kV with 40 mA target current. Data were collected from 5 to 80°. Raman spectra were used to identify the composition of the samples and the spectra were collected by a NT-MDT confocal Raman microscope and the exciting laser wavelength and laser spot size are 473 nm and ~500 nm, respectively. The data were recorded for 10 s for each sample. Si peak at 520 cm^{-1} was used as a reference for calibration in Raman characterization. Chemical configurations were determined by X-ray photoelectron spectroscope (XPS, Phi V5000). XPS measurements were performed with an Mg Kα X-ray source on the samples. The energy calibrations were made against the C 1s peak to eliminate the charging of the sample during analysis. Surface morphology of samples was examined with a field-emission scanning electron microscope (FESEM, JSM-6500F). Electrochemical polarization curves were recorded by AUTOLAB pontentiostat (PGSTAT 302N) with a scan rate of 5 mV/s in 0.5 M H_2SO_4 electrolyte. A three-electrode configuration was adopted for polarization and electrolysis measurements using an Ag/AgCl (3.0 mol/kg KCl) electrode as the reference electrode while a graphite rod was used as the counter electrode and the WS_2 samples as the working electrode. The bias voltages applied were then presented with the correction to the reversible hydrogen electrode (RHE).

3. Results and discussion

3.1. Spectroscopic characterization for WS_2 and MoS_2

The scanning electron microscopy (SEM) images in Fig. 1(b) show the morphology of the pristine carbon cloth as well as the WS_2/carbon cloth and MoS_2/carbon cloth electrodes prepared at 200 and 1000 °C, respectively. The pristine carbon cloth surface is smooth and the diameter is ~10 μm for each fiber, while the surface of the WS_2 or MoS_2 coated carbon cloth is relatively rough. For both materials, some nano-sized particles are observed on the surface when the thermolysis temperature is set at 1000 °C. The surfaces for the samples prepared at 200 °C are smoother than those at 1000 °C. The X-ray diffraction (XRD) analysis is performed to reveal the composition and crystalline structures of obtained MoS_2 and WS_2, as shown in Fig. 2(a) and (b) respectively. The signals from the carbon cloth are observed at 26.8° and 43.5° (marked as "C") for all samples. As shown in Fig. 2(a), the presence of (002) reflection peak at 2θ about 14.2° indicates the periodicity along the direction perpendicular to the planar structure of MoS_2. It is only observed for the MoS_2 samples produced at 1000 °C but not at a lower temperature. For the WS_2 samples prepared at the lower temperatures, i.e. 200 and 400 °C, a weak (002) reflection peak at 2θ about 14.3° is observed. As the thermolysis temperature increases, better crystallinity of WS_2 is observed and other crystalline orientations such as (004), (103), and (110) are also found. However, different from the MoS_2, the reflection peak for WO_3 are pronounced (marked

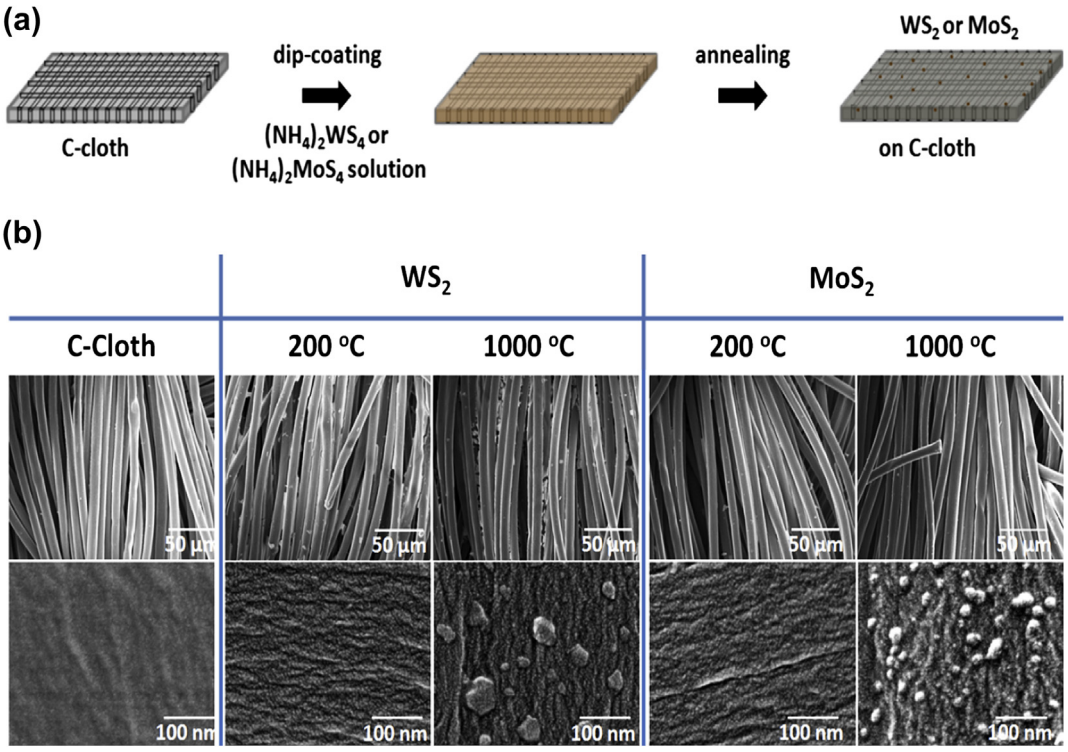

Fig. 1 – (a) Schematic illustration of the preparation of WS_2 and MoS_2 on carbon cloth electrode: Carbon cloth was used as the conducting substrate to load the precursors. After loading the precursors by immersion, carbon cloth was then baked on a hot-plate and then fed into a tube furnace for thermolysis, and (b) SEM images for pristine carbon clothes and those loaded with WS_2 and MoS_2 prepared by thermolysis at different temperatures.

with *) for the WS_2 samples prepared at 800 and 1000 °C. At such a high temperature, the trace amounts of oxygen in the CVD system react with the precursors, resulting in the formation of inevitable oxides. Note that there is no obvious MoO_3 formation for the MoS_2 samples prepared at high temperatures.

Raman spectra in Fig. 3(a) show that the characteristic peaks of MoS_2 including E_{2g} at 375 cm^{-1} and A_{1g} at 402 cm^{-1} [31]are observed for samples prepared at all temperatures and the peak intensity increases with the thermolysis temperature. By considering the information obtained from XRD in Fig. 2(a), it is concluded that amorphous MoS_2 is the major component in the sample prepared at lower temperatures and the content of crystalline MoS_2 component increases with the thermolysis temperature. Different from the case for MoS_2, Fig. 3(b) shows that the three vibration modes of WS_2, i.e. E_{1g} at ~298 cm^{-1}, E^1_{2g} at ~353 cm^{-1} and A_{1g} at ~418 cm^{-1} are observed for all the samples (200, 400, 800 and 1000 °C)

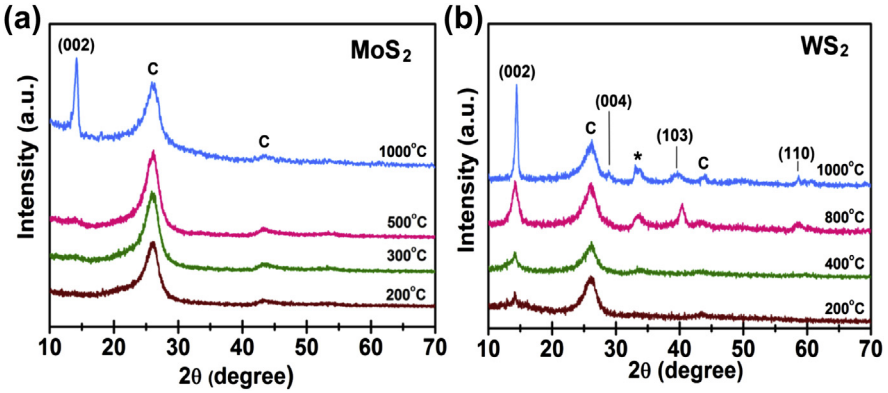

Fig. 2 – XRD pattern for the samples obtained at different thermolysis temperatures: (a) MoS_2 on carbon cloth and (b) WS_2 on carbon cloth. Peaks with notation C represent the carbon peaks from carbon cloth. (*) indicates the peaks from WO_3.

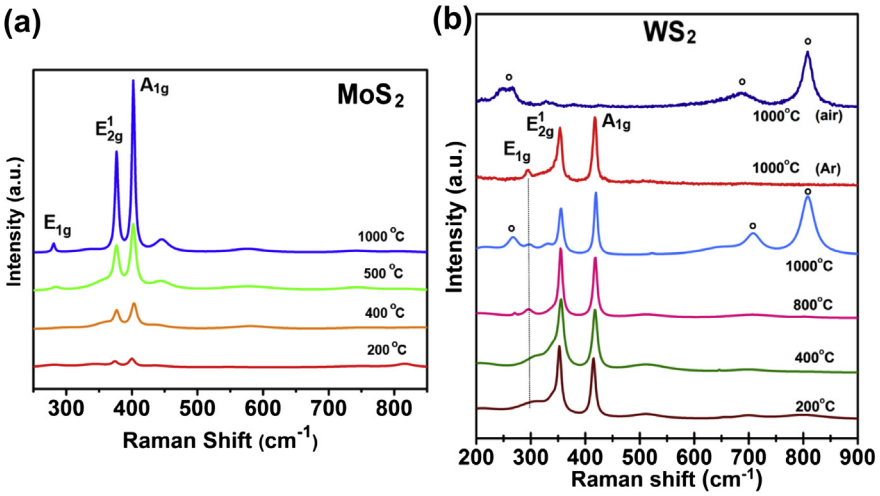

Fig. 3 – Raman spectrum of the samples with various preparation temperatures: (a) MoS_2 on carbon cloth and (b) WS_2 on carbon cloth. (o) indicates the peak for WO_3.

prepared in a standard environment ($Ar:H_2$ = 80 sccm:20 sccm). The top two curves are the reference samples prepared at 1000 °C respectively in air and in pure Ar. Note that the sample prepared in air is processed with very careful baking to move residual moisture in the DMF solvent and pumping/purging to reduce the presence of residual oxygen species in the CVD system prior to synthesis. It is clearly seen that the sample prepared in air exhibits characteristic O–W–O bending mode (~266 cm^{-1}) and broad stretching modes (centered at ~700 and 810 cm^{-1}), indicating the presence of WO_3 [32]. By contrast the sample prepared in pure Ar only shows the characteristic peaks of crystalline WS_2. It is noted that the sample prepared at 1000 °C in a standard Ar/H_2 condition shows obvious vibration peaks for WO_3, consistent with the XRD results in Fig. 2(b).

The X-ray photoelectron spectroscopy (XPS) analysis for both W $4f_{7/2\text{-}5/2}$ and S $2p_{3/2\text{-}1/2}$ spectra are shown in Fig. 4. For the crystalline WS_2 sample formed in pure Ar, the W $4f_{7/2\text{-}5/2}$ spectrum shows a peak doublet for W^{4+} (32.7–34.9 eV) and the sample prepared in air exhibits a peak doublet for W^{6+} (36.0–38.1 eV) of WO_3. For the WS_2 samples prepared at 200 °C, the W $4f_{7/2\text{-}5/2}$ spectrum can be fitted to several doublets, **A** for W^{4+} (32.8–35.0 eV) as in WS_2, **B** for W^{5+} (33.0–35.2 eV) in a mixed environment as in WS_3, and **C** for W^{6+} (35.9–38.0 eV) at oxygen-rich surrounding for tungsten atoms as in WO_3. This observation is also confirmed by the S $2p_{3/2\text{-}1/2}$ spectrum shown in Fig. 4(b), where **E** peaks correspond to the S^{2-} in WS_2 (162.0–163.1 eV), and the two partially overlapping doublets attributed to S^{2-} on the low energy side (shown as **D**; 161.4–162.6 eV) and to S_2^{2-} pairs on the high energy side, (shown as **F**; 163.7–164.6 eV) in a 2:1 ratio [33,34]. The XPS spectra obtained for the WS_2 samples prepared at 1000 °C can also be fitted to similar doublets with various peak area ratios between **A**, **B**, **C** and **D**, **E**, **F** as shown in Fig. 4. An extra pair of doublet corresponding to sulfone [35] was also found. Note that the WO_3 distribution in the samples prepared at a high temperature 1000 °C is not uniform; hence, the relative peak ratios between doublets vary with the locations of the sample. (See additional XPS results in Fig. S1 and Raman mapping in Fig. S2 for details). In general, comparing to the samples prepared at 200 °C, more WO_3 was revealed in the sample prepared at 1000 °C. The actual reason for the unfavorable formation of WO_3 in a pure Ar environment compared with the H_2/Ar environment is still not clear. One possible reaction pathway is that the H_2 reduced the WS_2 to element W and then oxidized in the ambient [36]. It might also be related to the different thermolysis mechanisms [37,38].

Similar fitted results for both Mo $3d_{5/2\text{-}3/2}$ and S $2p_{3/2\text{-}1/2}$ spectra obtained for MoS_2 prepared at different temperature. However, the XPS results for MoS_2 samples demonstrate that the similar **B** doublets for Mo^{5+} (233.1 and 229.6 eV) in a mixed environment as in MoS_3 are only observed in the samples prepared at a low temperature such as 200 °C [30,39]. The sample prepared at a temperature higher than 300 °C exhibits only Mo^{4+} doublets of MoS_2 without pronounced characteristic peaks from MoO_3 (Supporting Fig. S3).

3.2. *Electrocatalytic performance for water splitting*

Fig. 5(a) and (b) shows the polarization curves of MoS_2 and WS_2 on carbon cloth electrodes prepared at various temperatures, where the current density is defined as the measured current normalized by the geometrical area (or projected area) of the carbon cloth. The HER efficiency of the thermolysis-produced MoS_2 decreases dramatically with the increasing annealing temperature (or increasing crystallinity of MoS_2), which is consistent with the trend for MoS_2 grown on graphene reported in our previous study [30]. At low thermolysis temperature, Mo $3d_{3/2}$ and $3d_{5/2}$ binding energies at 233.1 and 230 eV revealed by XPS suggest the presence of Mo^{5+} ions [40–42]. Meanwhile, the bridging S_2^{2-} might exist in the compound due to observation of characteristic peaks of S $2p_{1/2}$ and $2p_{3/2}$ at 164.3 and 163.2 eV as shown in Fig. S1 [40,42]. These unsaturated sulfur atoms in these materials such as bridging S_2^{2-} could be related to the HER activity [15,18,19,30]. It is noted that several recent reports have hypothesized that

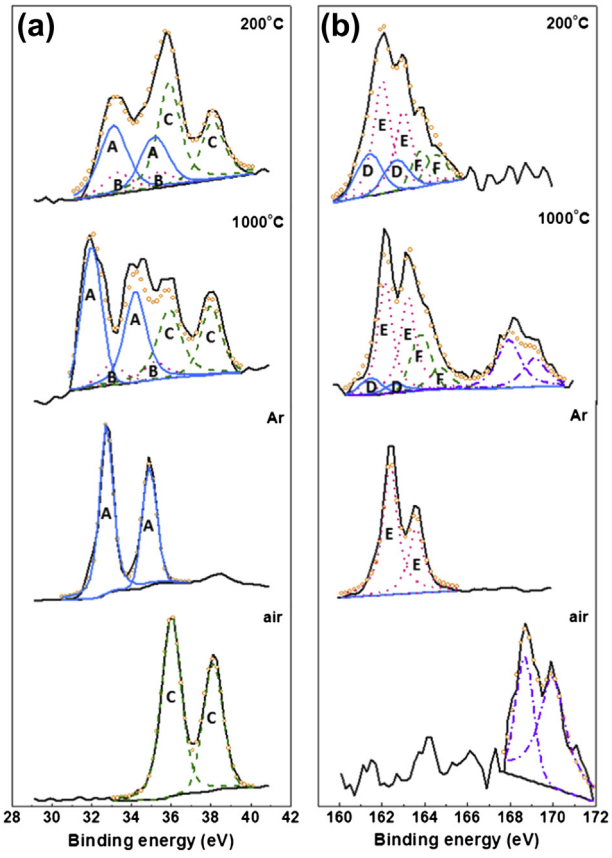

Fig. 4 – XPS analysis of (a) W $4f_{7/2\text{-}5/2}$ peaks and (b) S $2p_{3/2\text{-}1/2}$ for the sample thermolysis at 200 °C in Ar/H_2, 1000 °C in Ar/H_2, 1000 °C in Ar and 1000 °C in air. Doublet A is for W^{4+} as in WS_2, doublet B for W^{5+} in a mixed environment as in WS_3, and C for W^{6+} at oxygen-rich surrounding for tungsten atoms as in WO_3. Doublet E peaks correspond to the S^{2-} in WS_2 and the two partially overlapping doublets attributed to S^{2-} on the low energy side (D) and to S_2^{2-} pairs on the high energy side (F).

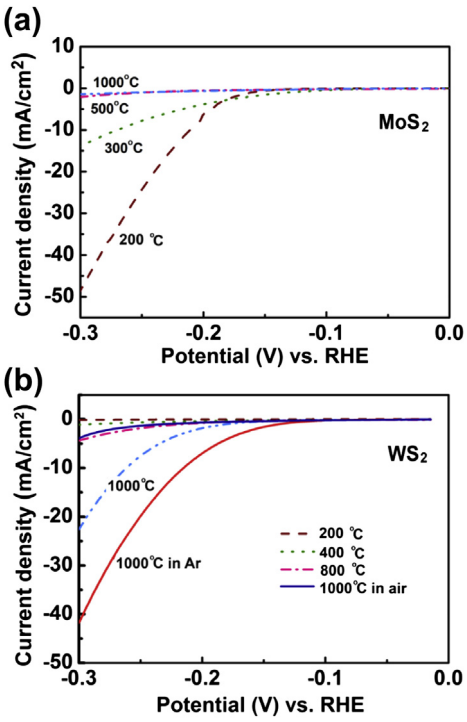

Fig. 5 – Polarization curves at a scan rate of 5 mV/s in 0.5 M H_2SO_4 electrolyte for (a) MoS_2 on carbon cloth and (b) WS_2 on carbon cloth obtained at the samples prepared at different temperatures and gas environments.

the amorphous MoS_2 might be also related to the HER reactivity in MoS_2 materials although the MoS_2 materials prepared in these reports were more defected or almost amorphous since no characteristic Raman A_{1g} and E^1_{2g} peaks were observed [18,39]. We can conclude from the above arguments that crystalline MoS_2 does not contribute to the HER. The unsaturated sulfur or amorphous MoS_2 play the key instead. Surprisingly, an opposite trend is noticed for WS_2/carbon cloth samples. Fig. 5(b) clearly shows that the HER efficiency increases with the thermolysis temperature. The current density for the WS_2 prepared at 1000 °C (in Ar/H_2 environment) is about 23 mA/cm^2 (at −300 mV vs. RHE), which is much better than the 0.01 mA/cm^2 for the WS_2 prepared at 200 °C. This may suggest that crystalline WS_2 is more active in HER although one might argue with the formation of WO_3 nanoparticles at the surface of the electrode might also have positive effect on HER. To test the hypothesis, we include the polarization curves for the two reference samples (prepared at 1000 °C in Ar and in air). The sample prepared in air, rich of WO_3 proved by XRD and Raman, shows a low HER efficiency. By contrast, the sample prepared in Ar demonstrates the best HER efficiency 42 mA/cm^2 (at −300 mV vs. RHE). These two samples clearly prove that the highly crystalline WS_2 sample is more active in HER.

The HER by electrocatalytic water splitting has been known to proceed by the following mechanisms, and each mechanism consists of two primary steps. The "discharge" step, the Volmer reaction (Eq. (1)), occurs in all cases, while either Heyrovsky reaction (Eq. (2)) or Tafel reaction (Eq. (3)) predominates to complete the reaction.

$$M + H_2O + e^- \rightleftharpoons M - H + OH^- \text{(Volmer reaction)} \quad (1)$$

$$M - H + H_2O + e^- \rightleftharpoons M + H_2 + OH^- \text{(Heyrovsky reaction)} \quad (2)$$

$$2M - H \rightleftharpoons 2M + H_2 \text{(Tafel reaction)} \quad (3)$$

where M is the catalyst active site. The catalytic performance of electrodes for HER can be described by Tafel relationship (Eq. (4)),

$$\eta = b\ln\left(\frac{i}{i_0}\right) \quad (4)$$

where η is the overpotential, i is the observed current density, and i_0 is the exchange current density. The Tafel slope b is the measurement of the potential increase required to enhance the resulting current density one order of magnitude. The exchange current density corresponds to the intercept at $\eta = 0$, extrapolated from a linear portion of Tafel plot. As a result, by analyzing the Tafel curves, the properties of various catalysts on HER can be revealed. The Tafel plots in Fig. 6 reveal a slope

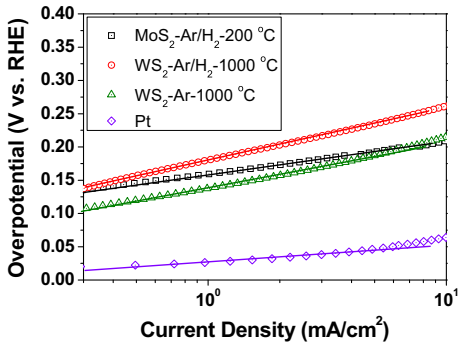

Fig. 6 – The comparison of WS_2 and MoS_2 on the Tafel plot. □ represents for MoS_2 thermolysis in Ar/H_2 at 200 °C, ○ for WS_2 thermolysis in Ar/H_2 at 1000 °C, △ for WS_2 thermolysis in Ar at 1000 °C and ◇ Pt.

of ca. 50 mV/dec for MoS_2, 78 mV/dec for the WS_2 prepared at 1000 °C, 68 mV/dec for the WS_2 prepared in Ar (1000 °C) and ca. 30 mV/dec for Pt for reference. A Tafel slope is an intensive parameter, which does not depend on the electrode surface area, and it is mainly due to the properties of the material such as hydrogen binding energy, the degree of crystallinity and so on. Note that the Tafel slope for the WS_2 prepared in air is 205 mV/dec (Supporting Fig. S4), corroborating that the WO_3 is not the HER active sites in the WS_2 prepared at 1000 °C. Moreover, based on DFT calculation, MoS_2 has the hydrogen binding energies of $\Delta G_H = 0.08$ eV for the Mo-edge site and $\Delta G_H = 0.18$ eV for the S-edge site but WS_2 has much larger hydrogen binding energies, where both S-and W-edges are equal to $\Delta G_H = 0.22$ eV [28]. As a result, the Tafel slopes for WS_2 are expected to be larger than MoS_2. We note that the Tafel slop for our MoS_2 prepared at 200 °C is 50 mV/dec, which is in between the 40 mV/dec from amorphous MoS_2 [18] and the 55–60 mV/dec from MoS_2 crystals [15], suggesting that the MoS_2 materials obtained in our process are likely a mixture of both. For our WS_2 materials prepared at 1000 °C, the Tafel slope is close to the 72 mV/dec from WS_2 crystalline nanosheets reported by Wu et al. [43], corroborating that the HER active sites of WS_2 are related to its crystalline structures. We have tabulated the HER Tafel slopes and exchange current density of MoS_2 and WS_2 obtained from this work and those available in literature (Supporting Table S1).

The durability of HER catalysts is also one of the most important factors. For MoS_2 serving as an electrocatalyst operating in acidic electrolytes, studies have done to prove the durability [17,30]. However, only a few studies focused on the durability of WS_2 related works [44]. Fig. 7 provides a three-hour-long HER test for the WS_2 prepared at 1000 °C with applied voltage of −200 mV vs. RHE. The current density for hydrogen evolution reaction is about 2.2 mA/cm^2 and it kept almost constant throughout the testing period in ambient. As a result, WS_2 can serve as an electrocatalyst in acidic solution as MoS_2.

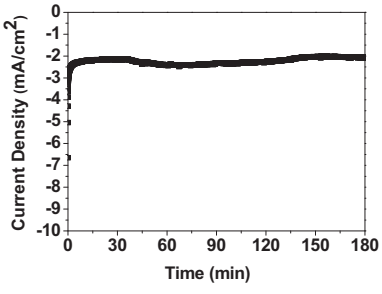

Fig. 7 – The durability test of WS_2 on carbon cloth with applied voltage of −200 mV vs. RHE over 180 min in 0.5 M H_2SO_4 electrolyte.

4. Conclusions

We have performed systematic studies on the catalytic reactivity of both MoS_2 and WS_2 materials produced by one-step and scalable CVD thermolysis process. It is observed that the high temperature-produced crystalline WS_2 is the active component for HER and it exhibits excellent stability in acidic electrolyte solutions. High temperature-produced WS_2 may serve for the applications requiring high thermal stability. By contrast, the HER activity for low temperature-produced MoS_2 is more active than its crystal form, and MoS_2 is thus a catalyst which can be produced with a simple and convenient preparative process. This work reveals the drastic difference of WS_2 and MoS_2 in HER behaviors and provides valuable information for further design of transition metal dichalcogenide catalysts.

Acknowledgments

This research was supported by Academia Sinica (IAMS and Nano program) and National Science Council Taiwan (NSC-99–2112-M-001–021-MY3). We also acknowledge the support from National Tsing Hua University, Taiwan.

Appendix A. Supplementary data

Supporting information are provided at http://www.sciencedirect.com. Supplementary data related to this article can be found at http://dx.doi.org/10.1016/j.ijhydene.2013.07.021.

REFERENCES

[1] Jeon HS, Permana ADC, Kim J, Min BK. Water splitting for hydrogen production using a high surface area RuO_2 electrocatalyst synthesized in supercritical water. Int J Hydrogen Energy. http://dx.doi.org/10.1016/j.ijhydene.2012.12.136.

[2] Abbaspour A, Norouz-Sarvestani F. High electrocatalytic effect of Au-Pd alloy nanoparticles electrodeposited on microwave assisted sol-gel-derived carbon ceramic electrode for hydrogen evolution reaction. Int J Hydrogen Energy 2013;38:1883–91.

[3] Kaninski MPM, Miulovic SM, Tasic GS, Maksic AD, Nikolic VM. A study on the Co-W activated Ni electrodes for

the hydrogen production from alkaline water electrolysis – energy saving. Int J Hydrogen Energy 2011;36:5227–35.
[4] Cross M, Varhue W, Pelletier K, Stewart M. RuO_2 nanorod coated cathode for the electrolysis of water. Int J Hydrogen Energy 2012;37:2166–72.
[5] Chiang CY, Epstein J, Brown A, Munday JN, Culver J, Ehrman S. Biological templates for anti reflective current collectors for photoelectrochemical cell applications. Nano Lett 2012;12:6005–11.
[6] Chiang CY, Chang MH, Liu HS, Tai CY, Ehramn S. Process intensification in the production of photocatalysts for solar hydrogen generation. Ind Eng Chem Res 2012;51:5207–15.
[7] Chiang CY, Shin Y, Aroh K, Ehrman S. Copper oxide photocathodes prepared by a solution based process. Int J Hydrogen Energy 2012;37:8232–9.
[8] Chiang CY, Shin Y, Ehrman S. Li doped CuO film electrodes for photoelectrochemical cells. J Electrochem Soc 2012;159:B227–32.
[9] Chiang CY, Aroh K, Franson N, Satsang VR, Dass S, Ehraman S. Copper oxide nanoparticles made by flame spray pyrolysis for photoelectrochemical water splitting – part II. Photoelectrochemical study. Int J Hydrogen Energy 2011;36:15519–26.
[10] Dresselhaus MS, Thomas IL. Alternative energy technologies. Nature 2001;414:332–7.
[11] Bard AJ, Fox MA. Artificial photosynthesis-solar splitting of water to hydrogen and oxygen. Acc Chem Res 1995;28:141–5.
[12] Walter MG, Warren EL, McKone JR, Boettcher SW, Mi Q, Santori EA, et al. Solar water splitting cells. Chem Rev 2010;110:6446–73.
[13] Greeley J, Jaramillo TF, Bonde J, Chorkendorff I, Norskov JK. Computational high-throughput screening of electrocatalytic materials for hydrogen evolution. Nat Mater 2006;5:909–13.
[14] Hinnemann B, Moses PG, Bonde J, Jørgensen KP, Nielsen JH, Horch S, et al. Biomimetic hydrogen evolution: MoS_2 nanoparticles as catalyst for hydrogen evolution. J Am Chem Soc 2005;127:5308–9.
[15] Jaramillo TF, Jorgensen KP, Bonde J, Nielsen JH, Horch S, Chorkendorff I. Identification of active edge sites for electrochemical H_2 evolution from MoS_2 nanocatalysts. Science 2007;317:100–2.
[16] Zong X, Yan H, Wu G, Ma G, Wen F, Wang L, et al. Enhancement of photocatalytic H_2 evolution on CdS by loading MoS_2 as cocatalyst under visible light irradiation. J Am Chem Soc 2008;130:7176–7.
[17] Li Y, Wang H, Xie L, Liang Y, Hong G, Dai H. MoS_2 nanoparticles grown on graphene: an advanced catalyst for the hydrogen evolution reaction. J Am Chem Soc 2011;133:7296–9.
[18] Merki D, Fierro S, Vrubel H, Hu XL. Amorphous molybdenum sulfide films as catalysts for electrochemical hydrogen production in water. Chem Sci 2011;2:1262–7.
[19] Merki D, Hu XL. Recent developments of molybdenum and tungsten sulfides as hydrogen evolution catalysts. Energy Environ Sci 2011;4:3878–88.
[20] Laursen AB, Kegnæs S, Dahl S, Chorkendorff I. Molybdenum sulfides-efficient and viable materials for electro-and photoelectrocatalytic hydrogen evolution. Energy Environ Sci 2012;5:5577–91.
[21] Tang ML, Grauer DC, Lassalle-Kaiser B, Yachandra VK, Amirav L, Long JR, et al. Structural and electronic study of an amorphous MoS_3 hydrogen-generation catalyst on a quantum-controlled photosensitizer. Angew Chem Int Ed Engl 2011;50:10203–7.
[22] Hou YD, Abrams BL, Vesborg PCK, Björketun ME, Herbst K, Bech L, et al. Bioinspired molecular co-catalysts bonded to a silicon photocathode for solar hydrogen evolution. Nat Mater 2011;10:434–8.
[23] Chen ZB, Cummins D, Reinecke BN, Clark E, Sunkara MK, Jaramillo TF. Core-shell MoO_3-MoS_2 nanowires for hydrogen evolution: a functional design for electrocatalytic materials. Nano Lett 2011;11:4168–75.
[24] Eda G, Yamaguchi H, Voiry D, Fuhita T, Chen M, Chhowalla M. Correction to photoluminescence from chemically exfoliated MoS_2. Nano Lett 2011;11:5111–6.
[25] Huang X, Zeng ZY, Zhang H. Metal dichalcogenide nanosheets: preparation, properties and applications. Chem Soc Rev 2013;42:1934–46.
[26] Lee YH, Zhang XQ, Zhang W, Chang MT, Lin CT, Chang KD, et al. Synthesis of large-area MoS_2 atomic layers with chemical vapor deposition. Adv Mater 2012;24:2320–5.
[27] Holt CMB, Murphy S, Gray MR, Mitlin D. Electrocatalytic hydrogenation of 2-cyclohexan-1-one in a high sulfur environment using a carbon-supported nanostructured tungsten sulfide catalyst. Catal Commun 2010;12:314–7.
[28] Bonde J, Moses PG, Jaramillo TF, Norskovb JK, Chorkendorff I. Hydrogen evolution on nano-particulate transition metal sulfides. Faraday Discuss 2008;140:219–31.
[29] Liu KK, Zhang W, Lee YH, Lin YC, Chang MT, Su CY, et al. Growth of large-area and highly crystalline MoS_2 thin layers on insulating substrates. Nano Lett 2012;12:1538–44.
[30] Chang YH, Lin CT, Chen TY, Hsu CL, Zhang W, Wei KH, et al. Highly efficient electrocatalytic hydrogen production by MoSx grown on graphene-protected 3-dimentional Ni foams. Adv Mater 2013;25:756–60.
[31] Lee C, Yan H, Brus LE, Heinz TF, Hone J, Ryu S. Anomalous lattice vibrations of single and few-layer MoS_2. ACS Nano 2010;4:2695–700.
[32] Rajeswari J, Kishore PS, Viswanathan B, Varadarajan TK. Hydrogen evolution reaction on WO_3 nanorods. Nanoscale Res Lett 2007;2:496–503.
[33] Khudorozhko GF, Asanov IP, Mazalov LN, Kravtsova EA, Parygina GK, Fedorov VE, et al. The study of electronic structure of molybdenum and tungsten trisulfides and their lithium intercalated by X-ray electron and X-ray emission and absorption spectroscopy. J Electron Spectrosc Relat Phenom 1994;68:199–209.
[34] Martin I, Vinatier P, Levasseur A, Dupin JC, Gonbeau D. XPS analysis of the lithium intercalation in amorphous tungsten oxysulfide thin films. J Power Sources 1999;81:306–11.
[35] Zhang GX, Sun SH, Yang DQ, Dodelet JP, Sacher E. The surface analytical characterization of carbon fibers functionalized by H_2SO_4/HNO_3 treatment. Carbon 2008;46:196–205.
[36] Zuckerman JJ, Hagen AP. Inorganic reactions and methodsIn The formation of bonds to hydrogen (part 1), vol. 1. VCH Publisher, Inc.; 1986. p. 143.
[37] Brito JL, Ilija M, Hernfindez P. Thermal and reductive decomposition of ammonium thiomolybdates. Thermochim Acta 1995;256:325–38.
[38] Xing PF, Zhai YC, Tian YW, Chao YS, Chen F. Kinetics of thermal decomposition of ammonium thiotungstate of granularity 62~72 μm in N_2. T Nonferr Metal Soc 1996;6:45–8.
[39] Benck JD, Chen Z, Kuritzky LY, Forman AJ, Jaramillo TF. Amorphous molybdenum sulfide catalysts for electrochemical hydrogen production: insights into the origin of their catalytic activity. ACS Catal 2012;2:1916–23.
[40] Weber T, Muijsers JC, vanWolput HJMC, Verhagen CPJ, Niemantsverdriet JW. Basic reaction steps in the sulfidation of crystalline MoO_3 to MoS_2 as studied by X-ray photoelectron and infrared emission spectroscopy. J Phys Chem 1996;100:14144–50.
[41] Wang HW, Skeldon P, Thompson GE. XPS studied of MoS_2 formation from ammonium tetrathiomolybdate solutions. Surf Coat Technol 1997;91:200–7.

[42] Vrubel H, Merki D, Hu X. Hydrogen evolution catalyzed by MoS_3 and MoS_2 particles. Energy Environ Sci 2012;5:6136–44.
[43] Wu ZZ, Fang BZ, Bonakdarpour A, Sun AK, Wilkinson DP, Wang DZ. WS_2 nanosheets as a highly efficient electrocatalyst for hydrogen evolution reaction. Appl Catal B Environ 2012;125:59–66.
[44] Zong X, Han JF, Ma GJ, Yan HJ, Wu GP, Li C. Photocatalytic H_2 evolution on CdS loaded with WS_2 as cocatalyst under visible light irradiation. J Phys Chem C 2011;115:12202–8.